THE EFFECT OF UNPARTICLE IN THE PROCESSES $e^+e^- \to \gamma\gamma$ AND $\gamma e^- \to U^\mu e^-$ WHEN THE e^+, e^- BEAMS ARE POLARIZED IN UNPARTICLE PHYSICS

DAO THI LE THUY[*] AND LE NHU THUC[†]

Hanoi National University of Education, 136 Xuan Thuy, Cau Giay, Hanoi, Vietnam

E-mail: [*]thuydtl@hnue.edu.vn; [†]thucln@hnue.edu.vn

Abstract. *We investigate the influence of unparticle physics on the positron-electron* (e^+e^-) *collider via the scalar unparticle* (U) *and electron* (e^-) *exchange. From computing the contribution of the unparticle exchange to the cross-section (CS) as well as evaluating the dependence of differential cross-section (DCS) on the scattering angle* (θ), *we calculate the production of vector unparticle* (U^μ) *in the photon-electron* (γe^-) *collider in* $s-$ *and* $t-$ *channels such as missing energy distribution. Besides, we also found that the polarization of the* e^+, e^- *beams also significantly contributes to the CS and DCS of the unparticle production.*

Keywords: scalar unparticle; vector unparticle; DCS; CS.

Classification numbers: 11.15.Tk; 14.80.-j.

I. INTRODUCTION

The attractive scenario for describing a possible scale-invariant hidden sector with a continuous mass distribution, which is described in terms of "unparticle" was proposed by Georgi [1]. This scale - invariant sector combined with the Standard Model (SM) through interactions of the form $\mathscr{O}_{UV}\mathscr{O}_{SM}$, where $\mathscr{O}_{UV}$ is an unparticle operator and $\mathscr{O}_{SM}$ is a SM operator. A concrete example that can support unparticle stuff was suggested by Banks-Zaks [2, 3], with a suitable number of massless fermions, theory attains a non-trivial infrared fixed point and a conformal field theory can be realized at low energy [4].

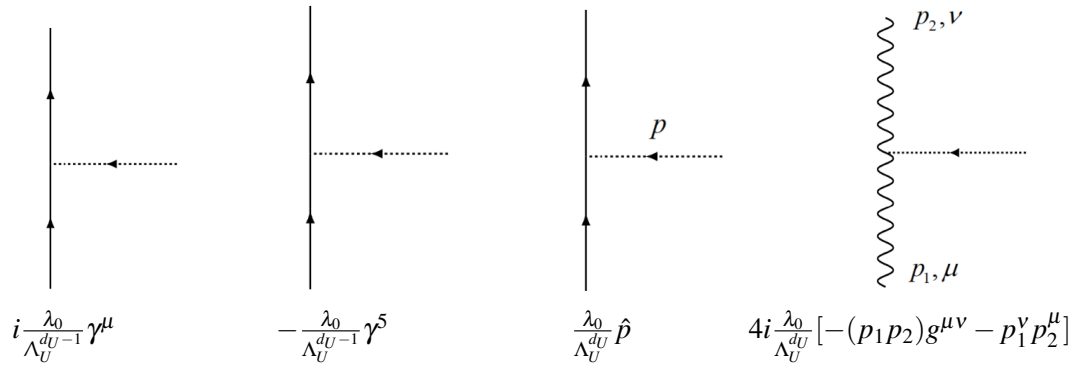The Lagrangian of the unparticle physics is as follows [4]

$$L = \frac{c_n}{M^{d_{UV}+n-4}} \mathcal{O}_{UV}\mathcal{O}_{SM}, \tag{1}$$

where M is the energy scale characterizing the new physics, the operator $\mathcal{O}_{UV}$ and operator $\mathcal{O}_{SM}$ have dimension d_{UV} and n, respectively and c_n is a dimensionless constant. In the low energy effective theory, the form of the operator is:

$$L = c_n \frac{\Lambda_U^{d_{UV}-d_U}}{M^{d_{UV}+n-4}} \mathcal{O}_U\mathcal{O}_{SM}, \tag{2}$$

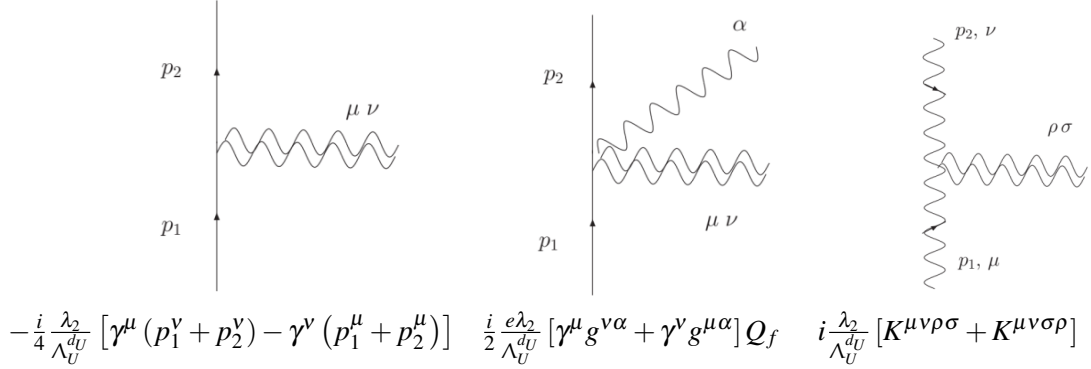where the unparticle operator $\mathcal{O}_U$ with a dimension d_U and an energy scale Λ_U.

Base on effective interactions between SM fields and the unparticles, the collider phenomenology of unparticle physics and Feynman rules for the scalar, vector, and tensor unparticle operators with SM fields are presented in Ref. [5]. The Feynman rules for the scalar, vector and tensor unparticle operators with SM fields are shown in Figs. 1, 2 and 3 [5]:

$$i\frac{\lambda_0}{\Lambda_U^{d_U-1}}\gamma^\mu \qquad -\frac{\lambda_0}{\Lambda_U^{d_U-1}}\gamma^5 \qquad \frac{\lambda_0}{\Lambda_U^{d_U}}\hat{p} \qquad 4i\frac{\lambda_0}{\Lambda_U^{d_U}}[-(p_1p_2)g^{\mu\nu}-p_1^\nu p_2^\mu]$$

Fig. 1. Feynman rules for the scalar unparticle operators.

$$i\frac{\lambda_1}{\Lambda_U^{d_U-1}}\gamma^\mu \qquad\qquad i\frac{\lambda_1}{\Lambda_U^{d_U-1}}\gamma^\mu\gamma^5$$
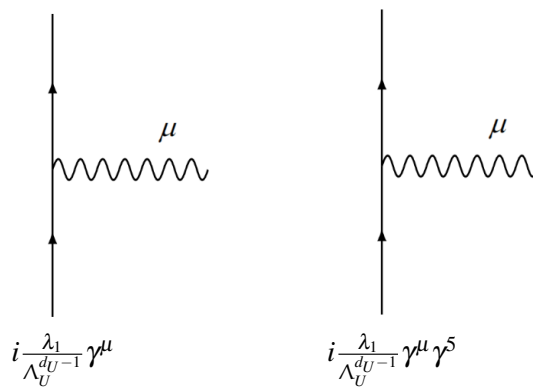
Fig. 2. Feynman rules for the vector unparticle operators.

$$-\frac{i}{4}\frac{\lambda_2}{\Lambda_U^{d_U}}\left[\gamma^\mu\left(p_1^\nu+p_2^\nu\right)-\gamma^\nu\left(p_1^\mu+p_2^\mu\right)\right] \qquad \frac{i}{2}\frac{e\lambda_2}{\Lambda_U^{d_U}}\left[\gamma^\mu g^{\nu\alpha}+\gamma^\nu g^{\mu\alpha}\right]Q_f \qquad i\frac{\lambda_2}{\Lambda_U^{d_U}}\left[K^{\mu\nu\rho\sigma}+K^{\mu\nu\sigma\rho}\right]$$

Fig. 3. Feynman rules for the tensor unparticle operators.

where λ_i are dimensionless effective couplings $C_{O_U^i}\Lambda_U^{d_{BZ}}/M^{d_{SM}+d_{BZ}-4}$ with the index $i=0,1,2$ labeling the scalar, vector, and tensor unparticle operators, respectively; $K^{\mu\nu\rho\sigma}=-g^{\mu\nu}p_1^\rho p_2^\sigma-(p_1 p_2)g^{\rho\mu}g^{\sigma\nu}+p_1^\nu p_2^\rho g^{\sigma\mu}+p_1^\mu p_2^\sigma g^{\rho\nu}$; Q_f denoting the charge of the fermion.

The propagators for scalar, vector, and tensor operators are given by [5]:

$$\Delta_F(P^2)=\frac{A_{d_U}}{2\sin(d_U\pi)}(-P^2)^{d_U-2}, \tag{3}$$

$$[\Delta_F(P^2)]_{\mu\nu}=\frac{A_{d_U}}{2\sin(d_U\pi)}(-P^2)^{d_U-2}\pi_{\mu\nu}(P), \tag{4}$$

$$[\Delta_F(P^2)]_{\mu\nu\rho\sigma}=\frac{A_{d_U}}{2\sin(d_U\pi)}(-P^2)^{d_U-2}T_{\mu\nu\rho\sigma}(P), \tag{5}$$

with

$$A_{d_U}=\frac{16\pi^2\sqrt{\pi}}{(2\pi)^{2d_U}}\frac{\Gamma(d_U+\frac{1}{2})}{\Gamma(d_U-1)\Gamma(2d_U)}, \tag{6}$$

$$\pi^{\mu\nu}(P)=-g^{\mu\nu}+\frac{P^\mu P^\nu}{P^2}, \tag{7}$$

$$T^{\mu\nu\rho\sigma}(P)=\frac{1}{2}\left\{\pi^{\mu\rho}(P)\pi^{\nu\sigma}(P)+\pi^{\mu\sigma}(P)\pi^{\nu\rho}(P)-\frac{3}{2}\pi^{\mu\nu}(P)\pi^{\rho\sigma}(P)\right\}. \tag{8}$$

Subsequently, many studies on unparticles have been done like that cosmology and astrophysics [6], black holes [7–9], and super-conductors [10–12]. The data analysis at LHC [13–16] is possible signatures of unparticle.

In the process of scattering to searching for the new physics effects, e^+e^- collision is one of the especially advantageous processes for its simple and clean background which the International Linear Collider (ILC) is designed for this linear electron-positron collision [17]. The photon collider (γe^-) is examined as an option of a linear electron-positron collider and possibilities of polarized e^+,e^- beams.

In this work, we studied the effect of scalar unparticle (U) and electron (e^-) exchange in $e^+e^-\to\gamma\gamma$ collision. The photons are produced from the $e^+e^-\to\gamma\gamma$ process maybe collide with the initial electron beams to produce vector unparticles(U^μ). In this paper, we were interested

in the production of U^μ from $\gamma e^- \to U^\mu e^-$ collision. In our study, we evaluated the dependence of the DCS on the scattering angle θ, and pointed the relevant direction to be able to observe unparticles. Besides, the CS was also considered as a function of the center of mass-energy $\sqrt{s}$.

II. THE COLLISION PROCESSES $e^+e^- \to \gamma\gamma$ AND $\gamma e^- \to U^\mu e^-$ IN UNPARTICLE PHYSICS

In this section, we investigate the influence of scalar unparticle in the e^+e^- collision process and study the production of the vector unparticle in the collision of an electron with the photon. The photon source could be the source from the previous e^+e^- collision, or an external laser source. Taking into calculating the cross-section, we can point out a beneficial direction for the unparticle signal. The above processes are described by Feynman diagrams through channels can be as follows:

The photon-photon production at e^+e^- colliders via scalar unparticle and electron (e^-) exchange is given by Fig. 4. According to the Feynman rules, we write the amplitudes of the s-, t- and u-channels in case of both the e^+, e^- beams are polarized as follows: Note that, we have not included the intermediate calculation steps here, we only give the final result of the scattering amplitude to support the numerical evaluation in the next section.
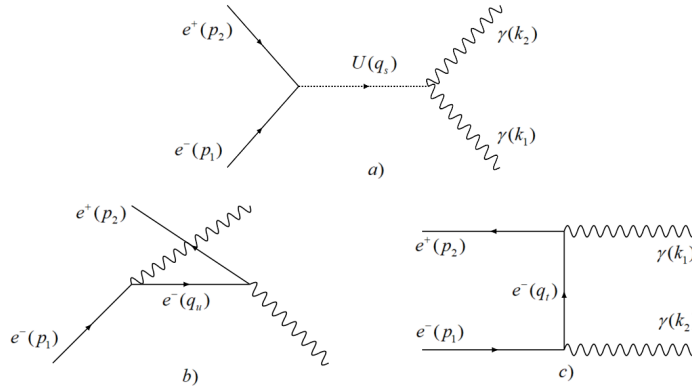
Fig. 4. The Feynman diagrams for the process $e^+e^- \to \gamma\gamma$.

For both the e^+ and e^- beams are left-polarized, the amplitude (M_{LL}) is:

$$M_{LL} = \frac{A_{d_U}}{2\sin(d_U\pi)}(-q_s^2)^{d_U-2}\left(4i\frac{\lambda_0}{\Lambda_U^{d_U}}(-(k_1 k_2)g^{\alpha\beta} + k_1^\beta k_2^\alpha)\right)\varepsilon_\alpha^*(k_1)\varepsilon_\beta^*(k_2)\frac{\lambda_0}{\Lambda_U^{d_U}}$$

$$\times \bar{v}(p_2,s_2)\hat{q}_s\frac{(1-\gamma^5)}{2}u(p_1,s_1) + \frac{i}{2}\frac{e^2}{q_u^2-m_e^2}\varepsilon_\mu^*(k_1)\varepsilon_\nu^*(k_2)\bar{v}(p_2,s_2)\gamma^\nu\hat{q}_u\gamma^\mu(1-\gamma^5)u(p_1,s_1)$$

$$+\frac{i}{2}\frac{e^2}{q_t^2-m_e^2}\varepsilon_\nu^*(k_1)\varepsilon_\mu^*(k_2)\bar{v}(p_2,s_2)\gamma^\nu\hat{q}_t\gamma^\mu(1-\gamma^5)u(p_1,s_1). \tag{9}$$

The case of both the e^+ and e^- beams are right-polarized, the amplitude (M_{RR}) is:

$$M_{RR} = \frac{A_{d_U}}{2\sin(d_U\pi)}(-q_s^2)^{d_U-2}\left(4i\frac{\lambda_0}{\Lambda_U^{d_U}}(-(k_1k_2)g^{\alpha\beta}+k_1^{\beta}k_2^{\alpha})\right)\varepsilon_{\alpha}^*(k_1)\varepsilon_{\beta}^*(k_2)\frac{\lambda_0}{\Lambda_U^{d_U}}$$

$$\times\bar{v}(p_2,s_2)\hat{q}_s\frac{(1+\gamma^5)}{2}u(p_1,s_1)+\frac{i}{2}\frac{e^2}{q_u^2-m_e^2}\varepsilon_{\mu}^*(k_1)\varepsilon_{\nu}^*(k_2)\bar{v}(p_2,s_2)\gamma^{\nu}\hat{q}_u\gamma^{\mu}(1+\gamma^5)u(p_1,s_1)$$

$$+\frac{i}{2}\frac{e^2}{q_t^2-m_e^2}\varepsilon_{\nu}^*(k_1)\varepsilon_{\mu}^*(k_2)\bar{v}(p_2,s_2)\gamma^{\nu}\hat{q}_t\gamma^{\mu}(1+\gamma^5)u(p_1,s_1). \tag{10}$$

In case of the e^+ beams are left-polarized, the e^- beams are right-polarized, the amplitude (M_{LR}) is:

$$M_{LR} = \frac{A_{d_U}}{2\sin(d_U\pi)}(-q_s^2)^{d_U-2}\left(4i\frac{\lambda_0}{\Lambda_U^{d_U}}(-(k_1k_2)g^{\alpha\beta}+k_1^{\beta}k_2^{\alpha})\right)(i-1)\frac{\lambda_0}{\Lambda_U^{d_U-1}}\varepsilon_{\alpha}^*(k_1)\varepsilon_{\beta}^*(k_2)$$

$$\times\bar{v}(p_2,s_2)\frac{(1+\gamma^5)}{2}u(p_1,s_1)+\frac{im_e}{2}\frac{e^2}{q_u^2-m_e^2}\varepsilon_{\mu}^*(k_1)\varepsilon_{\nu}^*(k_2)\bar{v}(p_2,s_2)\gamma^{\nu}\gamma^{\mu}(1+\gamma^5)u(p_1,s_1)$$

$$+\frac{im_e}{2}\frac{e^2}{q_t^2-m_e^2}\varepsilon_{\nu}^*(k_1)\varepsilon_{\mu}^*(k_2)\bar{v}(p_2,s_2)\gamma^{\nu}\gamma^{\mu}(1+\gamma^5)u(p_1,s_1). \tag{11}$$

For the e^+ beams are right-polarized, the e^- beams are left-polarized, the amplitude (M_{RL}) is:

$$M_{RL} = \frac{A_{d_U}}{2\sin(d_U\pi)}(-q_s^2)^{d_U-2}\left(4i\frac{\lambda_0}{\Lambda_U^{d_U}}(-(k_1k_2)g^{\alpha\beta}+k_1^{\beta}k_2^{\alpha})\right)\frac{\lambda_0}{\Lambda_U^{d_U-1}}(i+1)\varepsilon_{\alpha}^*(k_1)\varepsilon_{\beta}^*(k_2)$$

$$\times\bar{v}(p_2,s_2)\frac{(1-\gamma^5)}{2}u(p_1,s_1)+\frac{im_e}{2}\frac{e^2}{q_u^2-m_e^2}\varepsilon_{\mu}^*(k_1)\varepsilon_{\nu}^*(k_2)\bar{v}(p_2,s_2)\gamma^{\nu}\gamma^{\mu}(1-\gamma^5)u(p_1,s_1)$$

$$+\frac{im_e}{2}\frac{e^2}{q_t^2-m_e^2}\varepsilon_{\nu}^*(k_1)\varepsilon_{\mu}^*(k_2)\bar{v}(p_2,s_2)\gamma^{\nu}\gamma^{\mu}(1-\gamma^5)u(p_1,s_1). \tag{12}$$

From (9), (10), (11) and (12), we obtained the square of the amplitude elements above as follows:

$$|M_{LL}|^2 = |M_{RR}|^2$$

$$=32\left(\frac{A_{d_U}}{2\sin(d_U\pi)}(-q_s^2)^{d_U-2}\right)^2\left(\frac{\lambda_0}{\Lambda_U^{d_U}}\right)^4\left(2(k_1k_2)^2+k_1^2k_2^2\right)\left[2(p_1q_s)(p_2q_s)-(p_1p_2)q_s^2\right]$$

$$+\frac{1}{2}\left(\frac{e^2}{q_u^2-m_e^2}\right)^2\times16\left[2(p_1q_u)(p_2q_u)-q_u^2(p_1p_2)\right]$$

$$+\frac{1}{2}\left(\frac{e^2}{q_t^2-m_e^2}\right)^2\times16\left[2(p_1q_t)(p_2q_t)-q_t^2(p_1p_2)\right]$$

$$+ \frac{8A_{d_U}e^2}{\sin(d_U\pi)(q_u^2 - m_e^2)}(-q_s^2)^{d_U-2}\left(\frac{\lambda_0}{\Lambda_U^{d_U}}\right)^2\Big(2(k_1k_2)\big\{[(p_1q_s)(p_2q_u) - (p_1p_2)(q_sq_u) + (p_1q_u)(q_sp_2)]$$

$$+ p_1^2[(p_2k_1)(q_uk_2) - (p_2q_u)(k_1k_2) + (p_2k_2)(k_1q_u)] + p_2^2[(p_1k_1)(q_uk_2) - (p_1q_u)(k_1k_2) + (p_1k_2)(k_1q_u)]\big\}$$

$$+ \frac{8A_{d_U}e^2}{\sin(d_U\pi)(q_t^2 - m_e^2)}(-q_s^2)^{d_U-2}\left(\frac{\lambda_0}{\Lambda_U^{d_U}}\right)^2\Big(2(k_1k_2)\big\{[(p_1q_s)(p_2q_t) - (p_1p_2)(q_sq_t) + (p_1q_u)(q_sp_2)]$$

$$+ p_1^2[(p_2k_1)(q_tk_2) - (p_2q_t)(k_1k_2) + (p_2k_2)(k_1q_t)] + p_2^2[(p_1k_1)(q_tk_2) - (p_1q_t)(k_1k_2) + (p_1k_2)(k_1q_t)]\big\}$$

$$- \frac{32e^4}{2(q_u^2 - m_e^2)(q_t^2 - m_e^2)} \times \Big(\{(p_1q_u)(q_tp_2) - (p_1q_t)(q_up_2) + (p_1p_2)(q_uq_t)\}$$

$$+ 12\{(p_1q_u)(p_2q_t) - (p_1p_2)(q_uq_t) + (p_1q_t)(q_up_2)\}$$

$$+ 8\{(p_1p_2)(q_uq_t) - (p_1q_t)(p_2q_u) + (p_1q_t)(p_2q_u)\}\Big), \tag{13}$$

$$|M_{\text{LR}}|^2 = |M_{\text{RL}}|^2$$

$$= 64\left(\frac{A_{d_U}}{2\sin(d_U\pi)}(-q_s^2)^{d_U-2}\right)^2\left(\frac{\lambda_0}{\Lambda_U^{d_U-1}}\right)^2\left(\frac{\lambda_0}{\Lambda_U^{d_U}}\right)^2 \times \left(2(k_1k_2)^2 + k_1^2k_2^2\right) \times (p_1p_2)$$

$$+ \frac{16m_e^2}{2}\left(\frac{e^2}{q_u^2 - m_e^2}\right)^2(p_1p_2) + \frac{16m_e^2}{2}\left(\frac{e^2}{q_t^2 - m_e^2}\right)^2(p_1p_2)$$

$$- \frac{2e^2A_{d_U}m_e}{\sin(d_U\pi)}(-q_s^2)^{d_U-2}\frac{\lambda_0^2}{\Lambda_U^{2d_U-1}}\left(\frac{1}{(q_u^2 - m_e^2)} + \frac{1}{(q_t^2 - m_e^2)}\right)$$

$$\times [-4(k_1k_2)(p_1p_2) + \{(p_1p_2)(k_1k_2) - (p_1k_1)(p_2k_2) + (p_1k_2)(p_2k_1)\}]$$

$$+ \frac{16e^4m_e^2}{(q_u^2 - m_e^2)(q_t^2 - m_e^2)}(p_1p_2), \tag{14}$$

The corresponding Feynman diagrams for the pair production of the vector unparticle (U^μ) and electron in γe^- collider are shown in Fig. 5.

Fig. 5. The Feynman diagrams for the process $\gamma e^- \to U^\mu e^-$
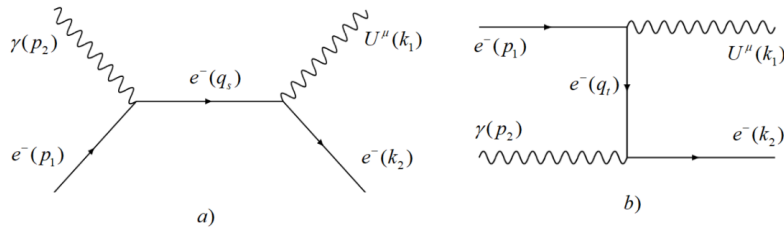
Similar to the above process, the amplitude of the s, t- channels in case of both the e^- initial and final beams are polarized, is given by:

- For both the e^- initial and final beams are left-polarized, the amplitude (M_{LL}) is:

$$
\begin{aligned}
M_{LL} =& \bar{u}_L(k_2,s_2)\, i\frac{\lambda_1}{\Lambda_U^{d_U-1}}\gamma^\nu\left(1+\gamma^5\right)\frac{-i\left(\hat{q}_s+m_e\right)}{q_s^2-m_e^2}\, ie\gamma^\mu u_L(p_1,s_1)\,\varepsilon_\nu^*(k_1)\,\varepsilon_\mu(p_2) \\
&+\bar{u}_L(k_2,s_2)\, ie\gamma^\nu\varepsilon_\nu(p_2)\frac{-i\left(\hat{q}_t+m_e\right)}{q_t^2-m_e^2}\varepsilon_\mu^*(k_1)\, i\frac{\lambda_1}{\Lambda_U^{d_U-1}}\gamma^\mu\left(1+\gamma^5\right)u_L(p_1,s_1) \\
=&0,
\end{aligned}
\tag{15}
$$

- For both the e^- initial and final beams are right-polarized, the amplitude (M_{RR}) is:

$$
\begin{aligned}
M_{RR} =& \frac{ie\lambda_1}{\Lambda_U^{d_U-1}\left(q_s^2-m_e^2\right)}\varepsilon_\nu^*(k_1)\,\varepsilon_\mu(p_2)\,\bar{u}(k_2,s_2)\,\gamma^\nu\left(1+\gamma^5\right)\hat{q}_s\gamma^\mu u(p_1,s_1) \\
&+\frac{ie\lambda_1}{\Lambda_U^{d_U-1}\left(q_t^2-m_e^2\right)}\varepsilon_\nu(p_2)\varepsilon_\mu^*(k_1)\bar{u}(k_2,s_2)\gamma^\nu(1+\gamma^5)\hat{q}_t\gamma^\mu u(p_1,s_1),
\end{aligned}
\tag{16}
$$

- For the e^- initial beam is left-polarized and the final beam is right-polarized. Note that, this case only happens in the s-channel and we have:

$$
M_{RL} = M_{sRL} = m_e\frac{ie\lambda_1}{\Lambda_U^{d_U-1}\left(q_s^2-m_e^2\right)}\varepsilon_\nu^*(k_1)\varepsilon_\mu(p_2)\bar{u}(k_2,s_2)\gamma^\nu(1+\gamma^5)\gamma^\mu u(p_1,s_1),
\tag{17}
$$

- For the e^- initial beam is right-polarized and final beam is left-polarized. Note that, this case only happens in the t-channel and we have:

$$
M_{LR} = M_{tLR} = m_e\frac{ie\lambda_1}{\Lambda_U^{d_U-1}\left(q_t^2-m_e^2\right)}\varepsilon_\nu(p_2)\varepsilon_\mu^*(k_1)\bar{u}(k_2,s_2)\gamma^\nu(1-\gamma^5)\gamma^\mu u(p_1,s_1).
\tag{18}
$$

From (16), (17) and (18), we obtained the following results:

$$
\begin{aligned}
|M_{RR}|^2 =& 32\left(\frac{e\lambda_1}{\Lambda_U^{d_U-1}}\right)^2\left[\frac{1}{(q_s^2-m_e^2)^2}\left\{2(p_1q_s)(k_2q_s)-q_s^2(p_1k_2)\right\}\right. \\
&\left.+\frac{1}{(q_t^2-m_e^2)^2}\{2(p_1q_t)(k_2q_t)-q_t^2(p_1k_2)\}-\frac{2}{(q_s^2-m_e^2)(q_t^2-m_e^2)}(p_1k_2)(q_sq_t)\right],
\end{aligned}
\tag{19}
$$

$$|M_{RL}|^2 = 32m_e^2 \left(\frac{e\lambda_1}{\Lambda_U^{d_U-1}(q_s^2-m_e^2)} \right)^2 (p_1 k_2), \tag{20}$$

$$|M_{LR}|^2 = 32m_e^2 \left(\frac{e\lambda_1}{\Lambda_U^{d_U-1}(q_t^2-m_e^2)} \right)^2 (p_1 k_2), \tag{21}$$

$$M_{RR}^+ M_{RL} = 32m_e^2 \left(\frac{e\lambda_1}{\Lambda_U^{d_U-1}} \right)^2 \left[\frac{-2}{(q_s^2-m_e^2)^2}(q_s k_2) + \frac{1}{(q_s^2-m_e^2)}\frac{1}{(q_t^2-m_e^2)}(k_2 q_t) \right] \tag{22}$$

$$M_{RR}^+ M_{tLR} = 32m_e^2 \left(\frac{e\lambda_1}{\Lambda_U^{d_U-1}} \right)^2 \left[\frac{1}{(q_s^2-m_e^2)(q_t^2-m_e^2)}(p_1 q_s) - \frac{2}{(q_t^2-m_e^2)^2}(p_1 q_t) \right] \tag{23}$$

$$M_{RL}^+ M_{LR} = -16m_e^4 \left(\frac{e\lambda_1}{\Lambda_U^{d_U-1}} \right)^2 \frac{1}{(q_s^2-m_e^2)(q_t^2-m_e^2)} \tag{24}$$

Next section, we evaluate the DCS as a function of $\cos\theta$ and CS depends on $\sqrt{s}$ in the center-mass frame.

III. NUMERICAL RESULTS AND DISCUSSIONS

In the center of mass system, we use the formula (25) to estimate the numerical values and evaluate the DCS and CS.

$$\frac{d\sigma}{d\Omega} = \frac{1}{64\pi^2 s} \frac{\left|\vec{k}_1\right|}{\left|\vec{p}_1\right|} |M_{fi}|^2, \quad d\Omega = d(\cos\theta)d\varphi. \tag{25}$$

When the two final particles are identical then the formula (25) is reduced by a factor $1/2$.

To study this work, we choose $\lambda_0 = 1$; $\lambda_1 = 1$; $\Lambda_U = 1$ TeV [5] and $\sqrt{s} = 3000$ GeV.

First, we evaluate the CS of the process $e^+e^- \to \gamma\gamma$ as a function of d_U(Fig. 6) and the DCS as a function of $\cos\theta$(Fig. 7).

Depending on the spin choice (scalar, vector, or tensor) a bound on d_U can be deduced from unitarity conditions [18]. The d_U is a continuous parameter and is not necessarily bound to integer values, unparticles would appear as fractional particles, for scalar $1 \leq d_U \leq 2$ (and, in the case of fermions: vector and tensor, $3/2 \leq d_U \leq 5/2$) [19]. In this task, the CS's of the process $e^+e^- \to \gamma\gamma$ as a function of d_U are plotted in Fig. 6.
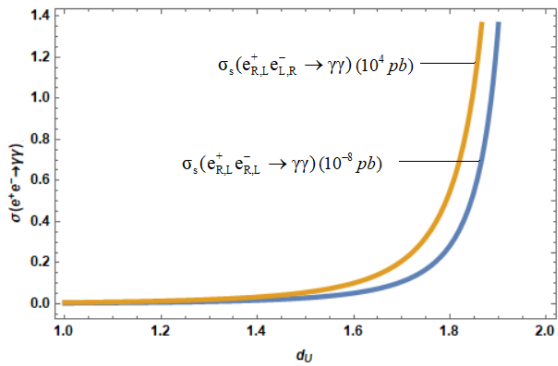
Fig. 6. The CS for $e^+e^- \to \gamma\gamma$ via U exchange (s-channel) as a function of d_U when the e^+, e^- beams are polarized.

For the process $e^+e^- \rightarrow \gamma\gamma$ via scalar unparticle exchange only happens in s-channel, the CS obtained has the same value in each of the following cases: both the e^+, e^- beams are left-polarized or right-polarized ($\sigma_s(e^+_{R,L}, e^-_{R,L} \rightarrow \gamma\gamma)$); the e^+ beams are left-polarized, e^- beams are right-polarized or vice versa ($\sigma_s(e^+_{R,L}, e^-_{L,R} \rightarrow \gamma\gamma)$). These results are shown in Fig. 6. In these cases, CS increases strongly when d_U increases from 1.7 to 1.9. This is the most interesting range for the influence of scalar unparticles during this collision. At $d_U = 1.9$, the CS has the values $\sigma_s(e^+_{R,L}, e^-_{R,L} \rightarrow \gamma\gamma) \approx 1.35 \times 10^{-8}$pb; $\sigma_s(e^+_{R,L}, e^-_{L,R} \rightarrow \gamma\gamma) \approx 2.61 \times 10^4 pb$.
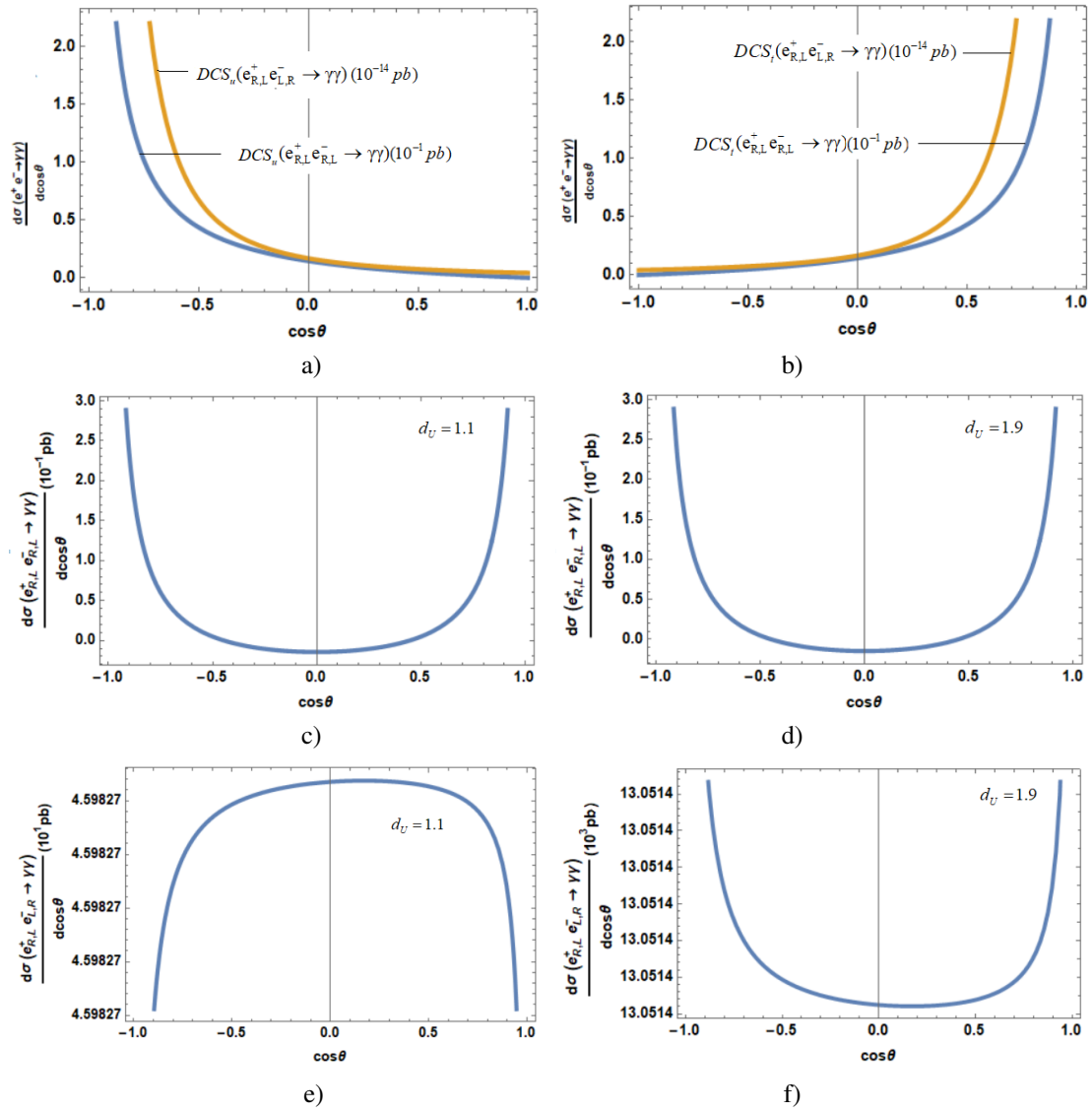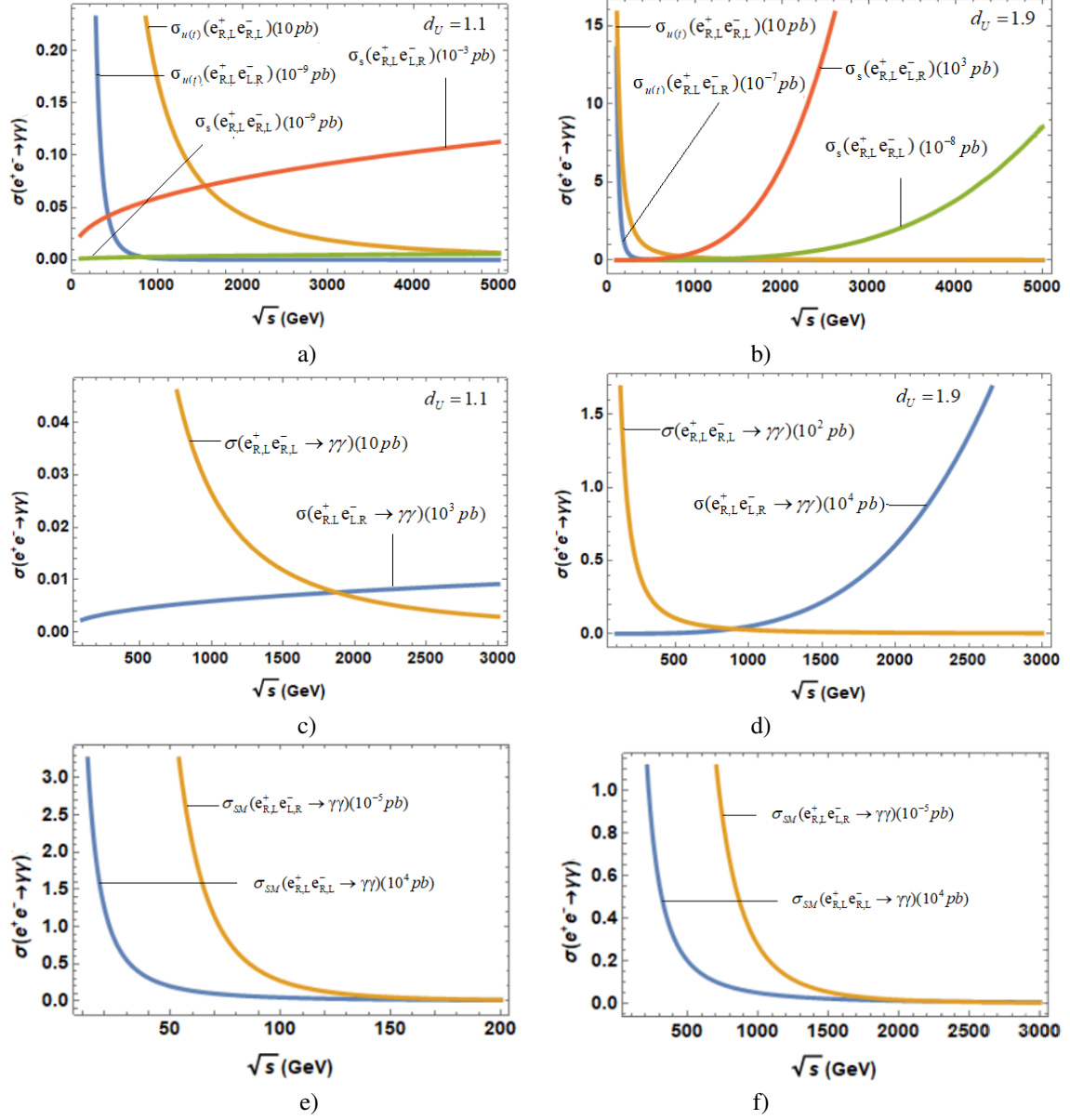

Fig. 7. The DCS for $e^+e^- \rightarrow \gamma\gamma$ as a function of $\cos\theta$.

Our next attention, the $\cos\theta$ dependence of DCS which is shown in Fig. 7 in the cases of polarized e^+, e^- beams. We see that: the DCS of the process $e^+e^- \to \gamma\gamma$ via e^- exchange depends very strongly on $\cos\theta$. The DCS decreases fast for u-channel (Fig. 7a), increases quickly for t-channel (Fig. 7b) when $\cos\theta$ is between -1 and 1. The DCS reaches the maximum value at $\cos\theta \approx -1.0$ for the u-channel and at $\cos\theta \approx 1.0$ for the t-channel. Remarkable thing: For s-channel, the DCS does not depend on the $\cos\theta$ and has the value $DCS_s(e^+_{R,L}, e^-_{R,L} \to \gamma\gamma) \approx 6.75 \times 10^{-9}$(pb), $DCS_s(e^+_{R,L}, e^-_{L,R} \to \gamma\gamma) \approx 1.31 \times 10^4 (pb)$ at $d_U = 1.9$; $DCS_s(e^+_{R,L}, e^-_{R,L} \to \gamma\gamma) \approx 2.37 \times 10^{-11}$(pb), $DCS_s(e^+_{R,L}, e^-_{L,R} \to \gamma\gamma) \approx 4.6 \times 10^1 (pb)$ at $d_U = 1.1$. However, when the phases are associated with all s-, t- and u- channels, the DCS is shown in Figs. 7 c, d, e, f, we can see that, in the case of both the e^+, e^- beams are left-polarized or right-polarized (Figs. 7 c,d) the DCS has the same result when $d_U = 1.1$ and $d_U = 1.9$, meanwhile, for the case of the e^+ beams are left-polarized, e^- beams are right-polarized or vice versa, the DCS changes negligible and have a different form when $d_U = 1.1$ and $d_U = 1.9$(Figs. 7 e,f). In particular, the DCS converges at the $\cos\theta = 0$ with $d_U = 1.1$ (see Fig. 7 e). This shows that the influence of d_U, as well as the polarization of e-beams on the DCS, are very important in investigating the behavior of the unparticle, it tells us the direction favored by the signal of the unparticle by experiment. In the SM, when the e^+, e^- beams are polarized, the DCS for the $e^+e^- \to \gamma\gamma$ process has been shown in Figs. 7 g, h. We can see, the DCS when e^+, e^- beams are both left polarized or right polarized is larger than the DCS in the case when e^+, e^- beams are polarized differently. In addition, in the low-energy region, the DCS of the process $e^+e^- \to \gamma\gamma$ is much larger than the DCS in the high-energy region.

In our next task, in Fig. 8, we plot the integrated DCS versus the $\sqrt{s}$ with 200 GeV$\leq \sqrt{s} \leq$ 3000 GeV, this is the energy that can be tested on ILC. The obtained CS has the identical value in the case of u-channel or t-channel. The CS decreases for u-, t- channels and increases for s-channel while $\sqrt{s}$ increases (Figs. 8a, 8b). The total CS in the case of associating with all s-, t- and u- channels (Fig. 8c and Fig. 8d) decreases when both the e^+, e^- beams are left-polarized or right-polarized and increases when the e^+ beams are left-polarized, e^- beams are right-polarized or vice versa. Thus, the cross-section of the process $e^+e^- \to \gamma\gamma$ via the scalar unparticle exchange increases when $\sqrt{s}$ increases. The contribution of the scalar unparticle (s- channel) is much larger than the contribution of the electron (u, t-channels).

For the scalar unparticle exchange contribution (s-channel), the obtained CS in the case of the e^+, e^- beams with the same polarization is much smaller than when the e^+, e^- beams are polarized differently. For the electron exchange contribution (u-, t-channels), the obtained CS in the case of the e^+, e^- beams the same polarization is much larger than when the e^+, e^- beams are polarized differently. However, the obtained total CS in the case of the e^+, e^- beams with different polarization is the largest when $d_U = 1.9$. In the high-energy region, the scalar unparticle exchange contribution is mainly in the process $e^+e^- \to \gamma\gamma$.

In the SM, unlike with the participation of scalar unparticles, the process $e^+e^- \to \gamma\gamma$ is only performed via the u- and t-channels (not via the s-channel). When the e^+, e^- beams are polarized, the dependence of the cross-section on $\sqrt{s}$ is shown as in Figs. 8 e, f. We can see, the cross-section of this process decreases when $\sqrt{s}$ increases. Besides that, we can also see the CS when e^+, e^- beams are both left polarized or right polarized is larger than the CS in the case when e^+, e^- beams are polarized differently (see Figs. 8e, 8f). This is contrary when there is the participation
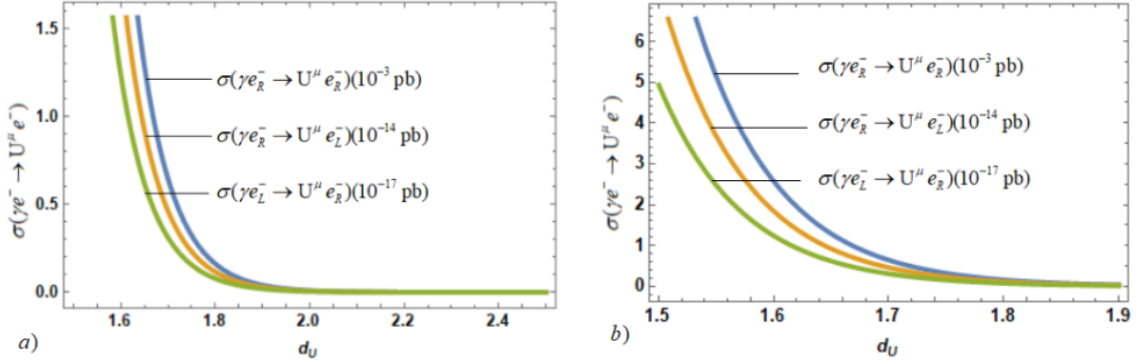
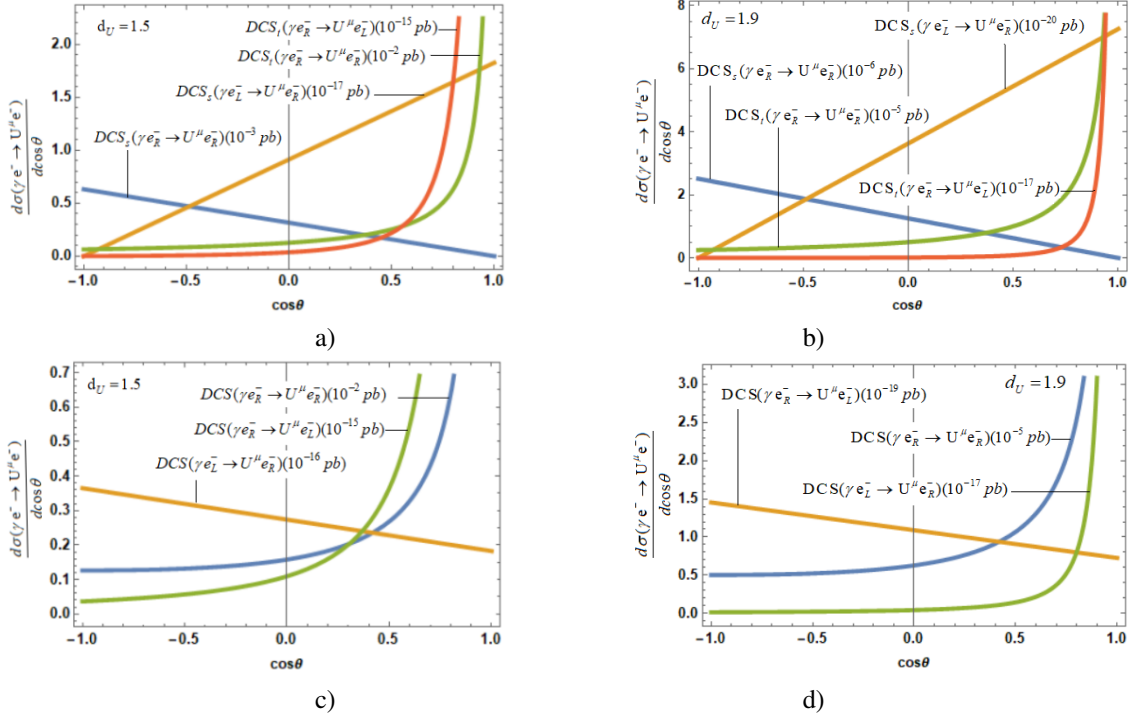**Fig. 8.** The CS for $e^+e^- \to \gamma\gamma$ as a function of $\sqrt{s}$.

of the scalar unparticles (see Figs. 8c, 8d). Thus, when the contribution of the scalar unparticles, the value of the cross-section of the process $e^+e^- \to \gamma\gamma$ has been changed.

Next to our part, we considered the process $\gamma e^- \to U^\mu e^-$ when the initial and final e^- beams are polarized. In Fig. 9 shows the d_U dependence of $\sigma(\gamma e^- \to U^\mu e^-)$. The $\cos\theta$ dependence of DCS($\gamma e^- \to U^\mu e^-$) is shown in Fig. 10 and the $\sqrt{s}$ dependence of $\sigma(\gamma e^- \to U^\mu e^-)$ is shown in Fig. 11. Here we plotted the dependence of $d_U, \cos\theta, \sqrt{s}$ on the CS of the process $\gamma e^- \to U^\mu e^-$
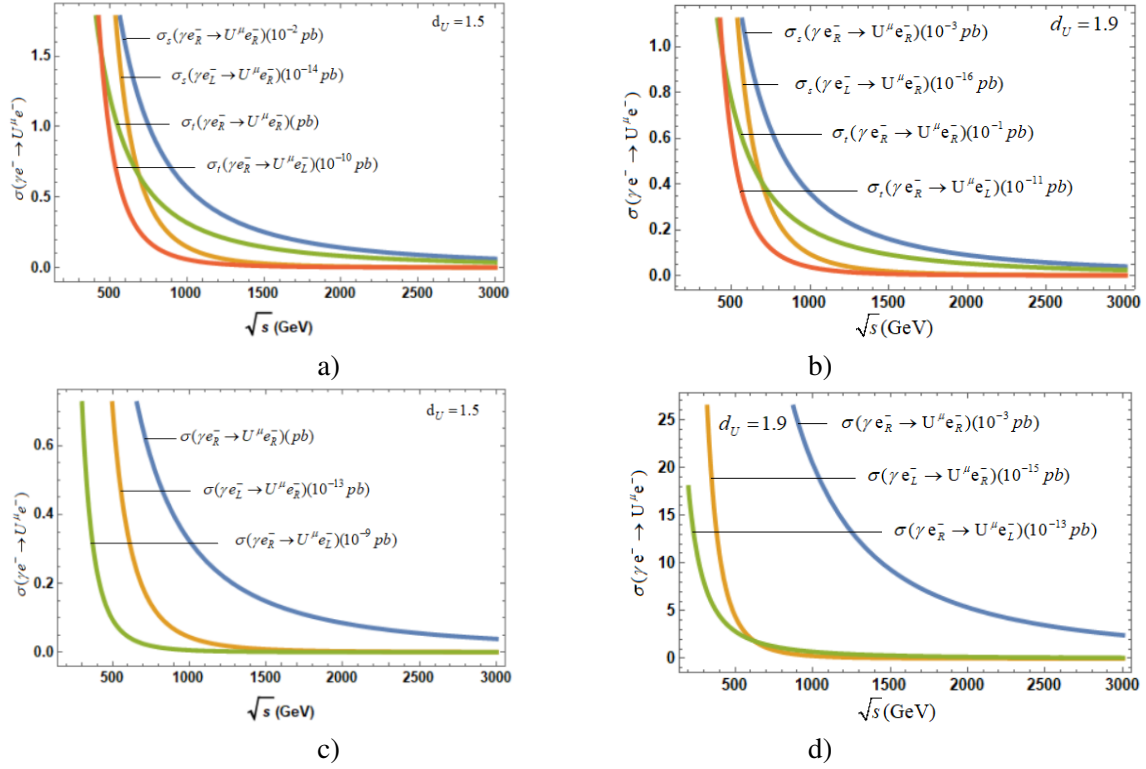
for both right-polarized initial and final e^- beams (s-, t-channels, $\gamma e_R^- \to U^\mu e_R^-$); right-polarized initial e^- beam, left-polarized final e^- beam (t-channel, $\gamma e_R^- \to U^\mu e_L^-$); left-polarized initial e^- beam, right-polarized final e^- beam (s-channel, $\gamma e_L^- \to U^\mu e_R^-$). In the case of both left-polarized initial and final e^- beams ($\gamma e_L^- \to U^\mu e_L^-$), the CS has the value zero.

Fig. 9. The cross-section for $\gamma e^- \to U^\mu e^-$ via U exchange (s-channel) as a function of d_U when the e^+, e^- beams are polarized.

Fig. 10. The DCS for $\gamma e^- \to U^\mu e^-$ as a function of $\cos\theta$

Fig. 11. The CS for $\gamma e^- \to U^\mu e^-$ as a function of $\sqrt{s}$.

Fig. 9 shows that the CS decreases strongly while $1.5 \le d_U \le 1.8$. The CS is much smaller for $1.8 \le d_U \le 2.5$. So that, we evaluated the DCS, CS of $\gamma e^- \to U^\mu e^-$ as a function of $\cos\theta$ or $\sqrt{s}$ at $d_U = 1.5$, $d_U = 1.9$.

For the s-channel, the DCS is a linear function of $\cos\theta$. For the t-channel, the DCS increases when $\cos\theta$ is from -1 to 1. For both right-polarized initial and final e^- beams in the t-channel, the DCS has a very much bigger value than the DCS for initial and final e^- beams are polarized differently. In this case, the DCS has the maximum value at $\cos\theta \approx 1$.

The $\sqrt{s}$ dependence of the CS of $\gamma e^- \to U^\mu e^-$ is shown in Fig. 11. Figs. 11a, and 11b had been plotted for each u -, and t- channel; Figs. 11c, and 11d had been plotted for the simultaneous contribution of both u -, t- channels. Where we see that, the CS decreases while $\sqrt{s}$ increases from 200 GeV to 3000 GeV in all cases polarized initial and final e^- beams. In the case of both right-polarized initial and final e^- beams, the obtained CS is the biggest (see Fig. 11c for $d_U = 1.5$, and Fig. 11d for $d_U = 1.9$). From Fig. 11c we also see that the $\sigma(\gamma e_R^- \to U^\mu e_L^-)$ (at the order of $10^{-9}pb$) and the $\sigma(\gamma e_L^- \to U^\mu e_R^-)$(at the order of $10^{-13}pb$) are very small compared to the $\sigma(\gamma e_R^- \to U^\mu e_R^-)$ (at the order of $1pb$), because of in the analytic expressions from (19) to (24), only the case of both right-polarized initial and final e^- beams is not proportional to the term m_e^2 (see Exp. 19). The remaining cases are all proportional to the terms m_e^2 or m_e^4. This is the same as for Fig. 11d.

At $\sqrt{s} = 200$ GeV, the CS has a value of about $18 \times 10^2 pb$ with $d_U = 1.5$ and about $2.86 \times 10^{-2} pb$ with $d_U = 1.9$. At $\sqrt{s} = 3000$ GeV, the CS has value about $9.7 pb$ with $d_U = 1.5$ and about $1,54 \times 10^{-4} pb$ with $d_U = 1.9$.

The unparticle production is the same as the missing energy signature. The final electron plus missing energy via the process $\gamma e^- \to U^\mu e^-$ in the low-energy region is much bigger than in the hight-energy region. So we hope that experiments will give more information about the unparticle production in the low-energy region.

IV. CONCLUSION

In high-energy region, the scalar unparticle exchange contribution is mainly in the process $e^+e^- \to \gamma\gamma$ in the case of the e^+, e^- beams are polarized differently and the influence of d_U, as well as the polarization of e^+, e^- beams on the cross-section, are very important in investigating the behavior of the unparticle, it tells us the direction favored by the signal of the unparticle by experiment.

The cross-section of the process $\gamma e^- \to U^\mu e^-$ is biggest when both initial and final e^- beams are right-polarized. In the high-energy region, the missing energy signature is much smaller than in the low-energy region, this results may be contributed to experiment in researching unparticles in γe^- collider in the low-energy region.

REFERENCES

[1] H. Georgi, *Phys. Rev. Lett.* **98** (2007) 221601.
[2] T. Banks, A. Zaks, *Nucl. Phys. B* **169** (1982) 189.
[3] CMS Collaboration, *Phys. Rev. D* **93** (2016) 052011.
[4] T. Kikuchi, N. Okada, *Phys. Lett. B* **661** (2008) 360.
[5] K. Cheung, W.Y. Keung and T. C. Yuan, *Phys. Rev. D* **76** (2007) 055003.
[6] H. Davoudiasl, *Phys. Rev. Lett.* **99** (2007) 141301.
[7] J. R. Mureika, *Phys. Lett. B* **660** (2008) 561–566.
[8] J. R. Mureika, *Phys. Rev. D* **79** (2009) 056003.
[9] J. R. Mureika and E. Spallucci, *Phys. Lett. B* **693** (2010) 129.
[10] J. P. F. LeBlanc and A. G. Grushin, *New J. Phys.* **17** (2015) 033039.
[11] P. W. Phillips, B. W. Langley, J. A. Hutasoit, *Phys. Rev. B* **88** (2013) 115129.
[12] K. Limtragool, P. Phillips, *Phys. Rev. B* **92** (2015) 155128.
[13] CMS Collaboration, *Eur. Phys. J. C* **75** (2015) 235.
[14] CMS Collaboration, *Phys. Rev. D* **93** (2016) 052011.
[15] CMS Collaboration, *JHEP* **03** (2017) 061, [arxiv: 1701.02042].
[16] T.M. Aliev, S. Bilmes, M. Solmaz, and I. Turan, *Phys. Rev.D* **95**, 095005 (2017).
[17] V. I. Telnov, Optimization of the beam crossing angle at the ILC for e+e- and $\gamma\gamma$ collisions, *arXiv:1801.10471* [physics. acc-ph], 2018.
[18] B. Grinstein, K. A.Intriligator, and I. Z. Rothstein, *Phys. Lett. B* **662** (2008) 367–374, arXiv:0801.1140. doi:10.1016/j. physletb.2008.03.020.
[19] G. Cacciapaglia, G. Marandella and J. Terning, *JHEP* **02** (2009) 049, arXiv:0804.0424. doi:10.1088/1126-6708/2009/02/049.